Металлофиз. новейшие технол. / Metallofiz. Noveishie Tekhnol.
2008, т. 30, № 2, сс. 169–187
Оттиски доступны непосредственно от издателя
Фотокопирование разрешено только
в соответствии с лицензией

ЭЛЕКТРОННЫЕ СТРУКТУРА И СВОЙСТВА

PACS numbers: 71.20.-b, 71.28.+d, 73.22.-f, 78.70.En, 79.60.-i, 82.80.Ej, 82.80.Pv

Energy Redistribution of the Valence Electrons Due to Nanodispersion of Materials and Its Evidence as Determined by the Ultrasoft X-Ray Emission Spectra

Ya. V. Zaulychnyy, Yu. M. Solonin, O. O. Foya, O. Yu. Khyzhun, and O. Vasylkiv*

I. M. Frantsevych Institute for Problems of Materials Science, N.A.S.U.,
3 Krzhyzhanov'sky Str.,
UA-03680 Kyyiv-142, Ukraine
**ICYS, National Institute for Materials Science,*
1-1 Namiki, Tsukuba,
305-0044 Ibaraki, Japan

An investigation under equal experimental conditions of the ultrasoft x-ray emission bands of coarse-grained and nanosize powders of different materials reveals the narrowing of the spectra and changes of their shapes when decreasing powder size. As shown, this is a consequence of the energy redistribution of valence-electron states after the breaking of interatomic bonds under dispersion of the materials into nanosizes, when a number of surface atoms with broken bonds become commensurable with the number of atoms within the nanoparticles. The energy redistribution of electrons occupying mainly the π-bonding states is changed significantly due to the increasing curvature of the surfaces of carbon nanomaterials with the decrease of their sizes. As revealed, the specific narrowing of the x-ray emission bands representing electron states of some symmetry is proportional to occupancy of these states.

Дослідження в однакових експериментальних умовах ультрам'яких рентґенівських емісійних смуг крупних та нанорозмірних порошків ріжних матеріялів свідчить про звуження спектрів та зміну їх форми при зменшенні розміру порошків. Показано, що це є наслідком енергетичного перерозподілу валентних електронів в результаті розриву міжатомового зв'язку при дисперґуванні матеріялів до нанорозмірів, коли число поверхневих атомів із розірваними зв'язками стає порівнянним з числом атомів в об'ємі наночастинок. Енергетичний перерозподіл електронів, що заповнюють переважно π-зв'язуючі стани, суттєво змінюється при збільшенні кривини поверхні вуглецевих наноматеріялів в результаті зменшення їх розмірів. Встановлено, що питомі звуження рентґенівських емісійних смуг, котрі відображають енергетичний розподіл електронних

станів певної симетрії у сполуці, є пропорційними заселености цих станів. Исследования в одинаковых экспериментальных условиях ультрамягких рентгеновских эмиссионных полос крупных и наноразмерных порошков различных материалов свидетельствуют о сужении спектров и изменении их формы при уменьшении размера порошков. Показано, что это является следствием энергетического перераспределения валентных электронов в результате разрыва межатомных связей при диспергировании материалов до наноразмеров, когда число поверхностных атомов с разорванными связями становится сравнимым с числом атомов в объеме наночастиц. Энергетическое перераспределение электронов, которые заполняют преимущественно π-связующие состояния, существенно изменяется при увеличении кривизны поверхности углеродных наноматериалов в результате уменьшения их размеров. Установлено, что удельные сужения рентгеновских эмиссионных полос, отображающих энергетическое распределение электронных состояний определенной симметрии в соединении, пропорциональны заселенности этих состояний.

Key words: ultrasoft x-ray emission spectroscopy, electronic structure, chemical bonding, nanodispersion.

(Received July 16, 2007)

1. INTRODUCTION

The energy state and unique properties of nanosystems are determined mainly by a considerable contribution of an interatomic interaction of the surface and near-surface atoms. Therefore, a study of the energy distribution of the valence electrons (EDVE) directly involved in interatomic interactions in nanoparticles is of current importance. Because the number of atoms in nanoparticles with sizes of 10–100 nm is several times greater than in clusters with several hundreds of atoms, the theoretical calculations employing X_α-methods [1–5] do not represent the electronic structure of the nanoparticles adequately. Theoretical methods developed recently for calculations of the electronic structure of nanoparticles involving 10^3–10^6 atoms are rather complicated [6–8]. Admixtures chemisorbed on the surfaces of nanoparticles make great contributions to the parameters of the interactions of surface atoms when investigating the EDVE of nanoparticles by means of optical [9–11], x-ray photoelectron spectroscopy (XPS) [12–18] and x-ray absorption spectroscopy (XAS) [19–22] methods. Recrystallization and agglomeration of nanoparticles prevent purification of their surface by heating-up [23]. Ion etching essentially breaks the morphology of nanoparticles and removes a substantial part of them from the substrates. The adhesive contact of discontinuous thin films with the substrates affects their electronic structure.

Therefore, it is necessary to study the EDVE of nanoparticles in the

absence of chemical and adhesive interactions and at sufficiently low temperatures. It is possible using the mechanical adhesion of nanoparticles on cooled substrates (*i.e.*, under rubbing of the metals possessing high thermal conductivity, *e.g.*, Cu or Au) and employing excitation of the spectra reflecting the EDVE by the electron beam that purifies the nanoparticle surfaces from chemisorbed admixtures and does not heat-up the nanoparticles.

The x-ray ultrasoft emission spectroscopy (XRUSES) method satisfies all these conditions under the excitation of radiation by electrons with energies of 2.0 to 9.0 keV. Under such conditions, the depth of photon emission giving the main contribution to the spectra intensity does not exceed 10 atomic layers in the nanoparticles. The x-ray emission bands reflect the partial density of electronic states of different symmetries of all kinds of atoms of a compound under investigation.

Changes of the shapes of the x-ray emission C2*p*-like bands due to their narrowing at $I = 2I_{\max}/3$ (I is the intensity) were observed when studying the electronic structure of high-pressure phases particularly of nanodiamonds (with coherent scattering areas (CSA) of 2.0, 3.0 and 5.0 nm) obtained from a highly nonequilibrium carbonic plasma as a result of explosive detonation [24]. This narrowing magnitude increases with a decrease in the CSA. The above narrowing effect was confirmed rather recently on nanodiamonds [25]. An even greater effect of the narrowing and the changing shapes of the x-ray emission NK_α and BK_α bands reflecting the EDVE of the *p*-symmetry of nitrogen and boron, respectively, was revealed in investigations of blended BN nanopowders. The effect of NK_α narrowing exceeds by three times that for the BK_α band, and the value increases with decreasing nanoparticle sizes [26].

Subsequent XRUSES studies of the nanopowders of other compounds with different atomic-crystalline structures and chemical bonding types have revealed that the nanosize narrowing of the spectra was observed in all nanomaterials investigated by us because the contributions of the localized levels of the electronic states to the valence bands after the interatomic bond breaking become commensurable with the contributions of states involved into unbroken bonds.

Because the fine structure of the x-ray emission bands depends upon many crystal-chemical characteristics and its nanosize change becomes apparent in the different energy intervals of the valence bands, the aim of the present paper is (1) to show that the effect of narrowing and changes of the shapes of the ultrasoft x-ray emission bands (USXREB) reflecting the energy redistribution of the valence electrons is a common electronic-structural characteristic of a transition of materials from the bulk to a nanosize state and (2) to elucidate also the dependence of the above effect upon the type of chemical bonding and atomic-crystal structure.

Therefore, it is necessary to study and analyze the parameters of the USXREB obtained from the bulk and nanomaterials, among which there are following powders:

1) covalent-ionic graphite-like (*h*-BN) and blended-like (*c*-BN) crystal modifications of boron nitride;

2) metal-covalent isostructural crystal TiC and TiN compounds with different ionicity degrees of the interatomic bonds;

3) ionic-covalent TiO_2 and $BaTiO_3$ with rutile- and perovskite-like structures, respectively;

4) carbon nanomaterials with a high contribution of closed bonds in their total quantity (fullerenes, low-imperfect nanotubes) and of opened bonds (onions, high-imperfect nanotubes and nanofibres).

2. EXPERIMENTAL

All the mentioned at the end of the introduction section materials under consideration were well characterized in Refs. [27, 28]. The above characterizations employing x-ray diffraction analysis have revealed that all the samples under study are single-phase materials.

The ultrasoft x-ray emission CK_α, NK_α, OK_α, BK_α ($K \to L_{\mathrm{II,III}}$ transition) and TiL_α ($L_{\mathrm{III}} \to M_{\mathrm{IV,V}}$ transition) bands reflecting the energy distribution of the C2*p*-, N2*p*-, O2*p*- and B2*p*- and valence Ti*sd*-like states, respectively, in the studied materials were obtained using two RSM-500 spectrometers. The x-ray emission CK_α, NK_α, OK_α and TiL_α bands were derived using the RSM-500 spectrometer with a diffraction grating possessing 600 lines/mm and a radius of curvature of $R \approx 6$ m. In the RSM-500 spectrometer used for studies of the BK_α band, the dispersion element was a diffraction grating with 600 lines/mm and a radius of curvature of $R \approx 2$ m. In the both spectrometers, the detectors were secondary electron multipliers VEU-6 with CsI photocathodes.

Operating conditions of x-ray tubes in the present experiments were the following: accelerating voltage $U_a = 4$ kV and anode current $I_a = 10$ mA when studying the BK_α bands and $U_a = 5$ kV and $I_a = 5$ mA when measuring the CK_α, NK_α, OK_α and TiL_α bands. The spectrometer energy resolutions were 0.2 eV in the case of measuring the BK_α band and about 0.3 eV in the energy regions corresponding to the positions of the CK_α, NK_α, OK_α and TiL_α bands. Comparisons of the x-ray emission bands on a common energy scale were fulfilled taking into account data of XPS measurements of binding energies of the B1*s*, C1*s*, N1*s*, O1*s* and Ti2*p* core-level electrons.

The measurements were made in an ion-pumped chamber of an ES-2401 spectrometer having a base pressure less than $5 \cdot 10^{-8}$ Pa. In the mentioned spectrometer, the MgK_α radiation ($E = 1253.6$ eV) was used as a source of spectra excitation. The binding energy of (84.00±0.05) eV of the XPS Au4$f_{7/2}$ core-level spectrum was used as a reference.

3. RESULTS AND DISCUSSION

3.1. Dependence of Nanosize Narrowing and Changes of the Shapes of the USXREB Due to the Transition of Covalent-Ionic BN from the Bulk to a Nanostate upon the Crystal-Chemical Characteristics of Its Modifications

Analysis of the comparison of the CK_α and superimposed on a common energy scale the NK_α and BK_α emission bands [24, 26] with band-structure calculations of diamond and blended BN has shown that the nanosize narrowing is observed in the energy region where the sp^3-hybride states involved in the C–C- and B–N-bonds of bulk crystals are located.

Essential distinctions in nanosize narrowings and changes of the shapes of the x-ray emission CK_α, NK_α and BK_α bands in crystal-analogues, diamond and blended BN, are obviously accounted for by only the ionic component [29] of the B–N-interaction. In Ref. [26], a detailed analysis of the influence of chemical bonding ionicity on the nanosize effect of the band's narrowing was not carried out and a transfer of the electronic density from one atom to another one reflects substantially on the intensities of the corresponding spectra; therefore, it is of great importance to elucidate the specific contribution to the mentioned effect of the population of the nitrogen and boron energy levels localized after bond breaking. Taking into account the fact that the widths of the NK_α and BK_α bands of the bulk blended *c*-BN are different (Fig. 1, *a*), it is necessary to introduce the parameter of the specific narrowing of these bands in one or another part of the spectra. In this case, we chose the spectra width at $I_{\max}/2$. The specific narrowing is then $\eta = (\Delta E^{\,c}_{1/2} - \Delta E^{\,n}_{1/2})/\Delta E^{\,c}_{1/2}$, where $\Delta E^{\,c}_{1/2}$ is the energy width of the x-ray emission bands at the half-maximum intensity in a coarse powder and $\Delta E^{\,c}_{1/2}$ is that in a nanopowder. The dependencies calculated in the present work for the η_{NK_α} and η_{BK_α} specific narrowing of the x-ray emission NK_α and BK_α bands upon the average sizes ($\bar{d}$) of *c*-BN powders (Fig. 1, *b*) were found to be linear with different coefficients k_{NK_α} and k_{BK_α}. Their ratios $\eta_{NK_\alpha}/\eta_{BK_\alpha} \approx 2.1 \pm 0.1$ were approximately equal for all fractions of the *c*-BN nanopowders.

The ratios were found to be close to the ratio $Q^{\,V}_{Np}/Q^{\,V}_{Bp} = 2.0$, where $Q^{\,V}_{Np}$ is the number of valence *p*-electrons located near one nitrogen atom and $Q^{\,V}_{Bp}$ is that near the boron atom, calculated in Ref. [29]. This indicates that the bigger the population of the levels of the atom emitting x-ray quanta the bigger is their contribution to the narrowing of the emission bands due to level's localization as a consequence of the disappearance of their splitting when the B–N-bonds break.

Because the EDVE [29] and the shapes of the x-ray emission NK_α and BK_α bands of *h*-BN and *c*-BN are different [30], the energy redistribution of the valence electrons should therefore be different on going

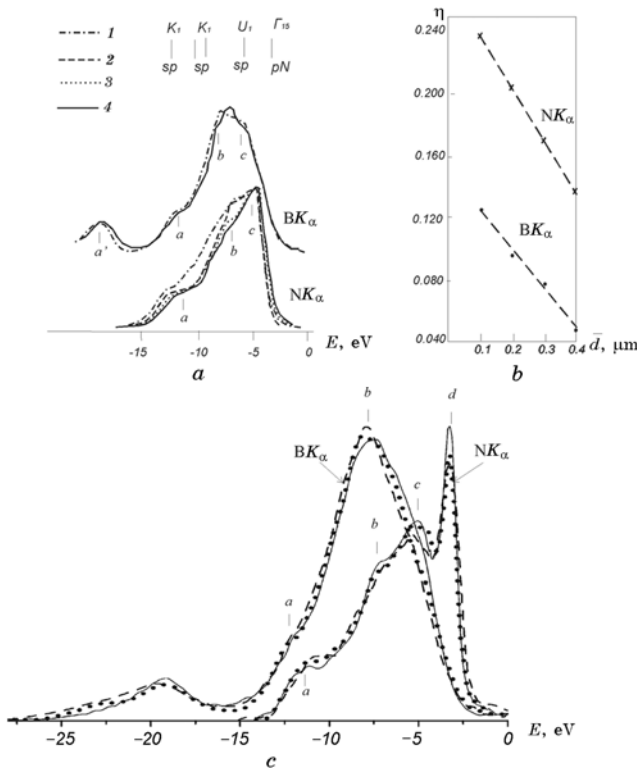

Fig. 1. Comparison of the x-ray emission NK_α and BK_α bands of *c*-BN powders with fraction sizes of 2.0 μm (dash-dotted curves *1*), 0.3 μm (dashed curve *2*), 0.2 μm (dotted curve *3*), 0.1 μm (solid curves *4*) (*a*) and the dependence of the specific narrowing of the bands upon the average size of *c*-BN particles (*b*); comparison of the x-ray emission NK_α and BK_α bands of coarse 5.0 μm (solid curves) and turbostratic 5.0 nm *h*-BN (dashed curves) powders (*c*): the dotted curves are the spectra of turbostratic *h*-BN (5.0 nm) heated by an electronic beam up to yellow-and-white luminescence of the particles ($T > 1500$ K evaluated by a pyrometer).

from coarse-grained *h*-BN to turbostratic *h*-BN (the average size of the latter particles is $\bar{d} = 5$ nm). Therefore, in the present paper for the first time, the NK_α and BK_α spectra of coarse-grained and turbostratic *h*-BN were investigated under the same conditions.

The number of the valence electrons and charge states of the atoms do not change as a result of ultradispersion (the binding energies of the core-level B1*s* and N1*s* electrons are invariable [27]); therefore, the BK_α bands, as well as the NK_α spectra, obtained from the coarse-grained and nanopowder BN were reduced to equal squares. From a comparison of these spectra on a common energy scale (Fig. 1, *c*), it is obvious that the BK_α bandwidth of turbostratic *h*-BN is smaller by

0.2–1.0 eV as compared with that of coarse *h*-BN in its high-energy part. In the energy region where the sp^2-hybrid states providing the B–Nσ-bonds are reflected, the intensity of the peculiarity *c* of the NK_α band decreases.

This is a result of the disappearance of splitting of B*p*- and N*p*-energy levels due to the dehybridization of a part of the sp^2-states after the breaking of B–N-bonds due to the nanodispersion of *h*-BN. The N*p*-dehybridizated states in turbostratic *h*-BN shift to the top of the valence band. This fact is reflected in the shift of the short-wave contour at the peak *d* of the NK_α band towards higher energies. From a comparison of the bandwidth reduction of *c*-BN (Fig. 1, *a*) and *h*-BN (Fig. 1, *c*), it is apparent that the BK_α bandwidth is reduced more in *h*-BN but the NK_α bandwidth is reduced more in *c*-BN.

This is explained obviously by the fact that in coarse *c*-BN all electrons, including those transferred to nitrogen, occupied the splitting levels of the sp^3-hybrid states whereas in *h*-BN the main part of the electrons occupies the weakly bonding Np_z-states reflected in the narrow peak *d* of the NK_α band [31]. The Np_z-states split weakly due to the low degree of π-overlapping with low-populated Bp_z-orbitals.

Therefore, in *h*-BN a smaller number of electrons are involved in splitting the sp^2-states as compared with that in *c*-BN. This fact is reflected in a smaller contribution to the emission of the NK_α band of the electrons involved in the dehybridized states. Thus from the above analysis, it is obvious that, during ultradispersion, the nearest surroundings essentially affect both the narrowing value and the changes of the shape of the USXREB representing the energy redistribution of the valence electrons.

3.2. Peculiarities of Nanosize Narrowing of the USXREB Obtained for Isostructural Metal-Covalent Titanium Carbides and Nitrides with a Face-Centred Cubic Lattice

In order to study a dependence of the effect of the nanosize narrowing of the USXREB upon the presence of the metallic component of the chemical bonding, we have analyzed the x-ray emission CK_α, NK_α and TiL_α bands obtained for three nanosize fractions and coarse powders of metal-covalent TiC and TiN [32, 33] with the face-centred cubic structure of the NaCl type. The $Fm3m$ space symmetry group of these compounds is close to those of diamond ($Fd3m$) and *c*-BN ($F43m$), but the quantity of the nearest neighbours and the geometry of the neighbourhoods are different. The measuring of widths of the CK_α, NK_α and TiL_α bands at $I_{max}/2$ of coarse and nanopowders with specific surface areas $S_{sp} = 9.4$, 16.8, 24.2 m^2/g for TiC [32] and $S_{sp} = 10$, 20, 50 m^2/g for TiN [33] and calculations of the specific narrowing of these bands have re-

vealed that the narrowing increases with decreasing fraction sizes. The specific narrowing of the CK_α and NK_α bands is greater than that of the TiL_α band, and their ratios are $\eta_{CK_\alpha}/\eta_{TiL_\alpha} \approx 1.3$ for TiC and $\eta_{NK_\alpha}/\eta_{TiL_\alpha} \approx$ ≈ 1.45 for TiN; whereas the ratios of the number of valence electrons near the constituent atoms calculated in Ref. [34] are $Q^V_{Cp}/Q^V_{Tisd} \approx 1.39$ (TiC) and $Q^V_{Np}/Q^V_{Tisd} \approx 1.64$ (TiN). These facts confirm the conclusion stated in section 3.1.

In metal-covalent TiN, in addition to the presence of the ionic component of the chemical bonding, the Fermi level passes through the high density of the metal-bonding band, where a significant part of the occupied anti-bonding states is also present [35]. In TiC, the number of valence electrons and the transfer of the electrons from titanium to carbon are smaller in comparison with those in TiN; therefore, the anti-bonding (Tisd + Cp)*-states are unoccupied and the Fermi level passes only through the minimum density of the metal-bonding states.

The analysis of a comparison of the x-ray emission CK_α, NK_α and TiL_α bands with data of theoretical calculations of the electronic structure of TiC and TiN [34] carried out in Refs. [32, 33] has shown that the band's narrowing occurs in the energy regions where hybrid-bonding Tisd + Xp-states (X = C, N) are located. In the energy range where the non-bonding states are mainly located, the widths of the both emission bands are not reduced, *i.e.* the contours of the bands of coarse-grained and nanopowder materials coincide. The TiL_α band narrows in low-energy and in high-energy regions due to the breaking of the covalent and metallic components of the bonds. The breaking of the metallic bonds leads to narrowing the TiL_α and CK_α bands in the near-Fermi region in TiC owing to the localization of levels of high-energy Tisd + Cp states delocalized in the lattice. These states provide the metallic component of the Ti–C interaction in TiC.

Because the electrons of the localized energy levels have to increase their energy after the bond breaking, their levels have to shift to the high-energy side and can locate in the energy region corresponding to the non-bonding states in a coarse powder. This can also be due to the fact that the high-energy contours of the CK_α band (Fig. 2, *a*) of coarse-grained and nanopowders of TiC coincide in the ΔE_2 energy range. In our opinion, the above effect is not visible in the case of TiN due to the superposition of the NK_α band and the TiL_l-line in this compound.

On the other hand, the short-wave contour at the main maximum d of the TiL_α band obtained from TiN (Fig. 2, *b*), due to the concentration in the energy region –(5.0–3.5) eV of the energy localized levels even shifted somewhat to the high-energy side after breaking the Ti–Ti- and Ti–N-bonds. Part of the hybrid K_4 (Cp_{x-y}, Ti$_y$), Δ_5 (C$p_{y,z}$, Ti$_{2g}$), $\sum_3$ (Cp_z, Ti$d_{z(x+y)}$) states is located in the above mentioned energy region in the bulk crystal according to the calculations [35]. Their splitting should also disappear during the bond breaking. The energy redistribution of

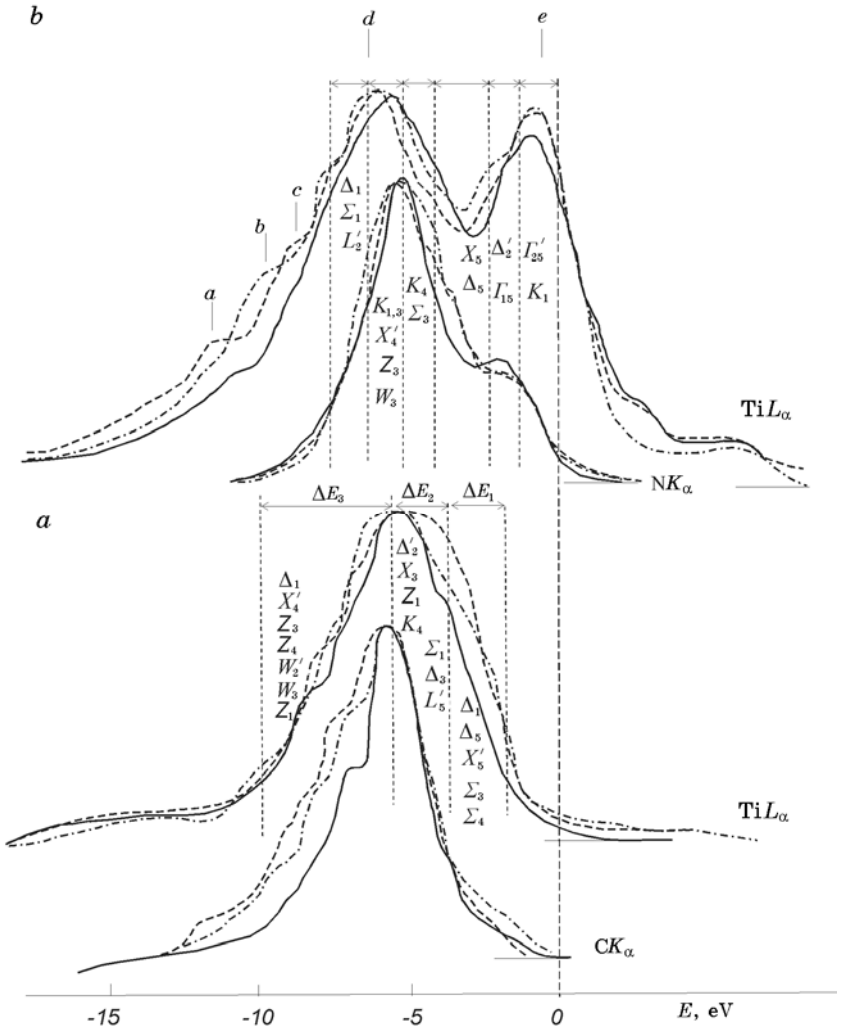

Fig. 2. Comparison of the x-ray emission TiL_α, CK_α and NK_α bands of coarse powders (dash-dotted curves), nanopowders (solid curves) and materials consolidated from the nanopowders at high-pressure and room temperature (dashed curves) of TiC (*a*) and TiN (*b*).

the metal-bonding Ti*sd*-states, which splitting disappeared after the bond breaking during the ultradispersion of TiN, is reflected by the smaller width and the intensity of the peak *e* of the TiL_α band. The redistribution shifts by 0.2–1.5 eV towards high energies the short-wave contour of the TiL_α band at $I < 0.4 I_{max}$.

It is worth mentioning that a high-energy shift by 0.4 eV of the whole short-wave contour of the x-ray emission NK_α band obtained

from the finest powder of *c*-BN as compared with that of the band of coarse *c*-BN was caused by a significant increase in the contributions of the occupied N*p*-like states corresponding to the broken bonds of atoms belonging to the large specific surface of *c*-BN nanopowders into the energy region corresponding to the top of the valence band. This fact shows that energy redistributions of the valence electrons as a result of the increasing energy of states involved in the broken bonds have some differences because of the ultradispersion of crystals with covalent and metallic bonds. The differences are the consequence of the different distributions and localizations of metal- and covalent-binding states within the valence bands as well as the different magnitudes of changes in energy states when the splitting of their energy levels disappears after braking the metallic and covalent bonds.

After the nanopowders' consolidation, crystallization and other processes, as a result of recombination of broken chemical bonds on the surface of the nanoparticles, the splitting of energy levels of the abovementioned electronic states should take place, and due to this fact, the USXREB should broaden.

Indeed, the x-ray emission CK_α, NK_α and TiL_α bands obtained from the nanopowders of solid TiC and TiN (Fig. 2) consolidated at 7 GPa and at room temperature (T = 293 K) were found to be broadened in the same energy regions where they were narrowed in the spectra of the nanopowders. This is a result of the energy levels splitting as a consequence of their orbital superimposition when drawing together surface atoms of contacting nanoparticles under the high-pressure contraction of the nanopowders.

3.3. Estimation of Band-Energy Changes as a Result of TiO_2 and $BaTiO_3$ Ultradispersion Using the Data for the Narrowing and Transformation of Shapes of the X-Ray Emission TiL_α and OK_α Bands

The elucidation of the dependence of the nanosize narrowing of the USXREB and energy redistributions of the valence electrons on the types of chemical bonding would be incomplete without a study of these effects in an ionic TiO_2 crystal with a rutile structure (r-TiO_2). In this crystal, the greater part of the occupied O*p*-states has to be nonbonding due to the big contribution to the cohesion energy of the Coulomb interaction between the titanium and oxygen ions. Therefore, in the present paper for the first time, the effect of nanosize narrowing of the x-ray emission TiL_α and OK_α bands was studied during the transition from a coarse powder to two fractions of nanopowders with average sizes of d = 107 and 10 nm (Fig. 3, *a*). Also for the first time, the broadening of the OK_α band (Fig. 3, *b*) of r-TiO_2 nanopowder (d = 10 nm) due to its recrystallization under heating (as a result of the rise from 8 to 45 W of the power of the electron beam exiting the spectra)

was investigated.

The valence band of coarse-grained r-TiO_2 contains mainly the Op-states. The bonding hybrid (Tid(e_g) + Op) states and the Op-states involved into the O–O-bonds contribute to the low-energy part, but the non-bonding Op-states are the main contributors to the high-energy part of the valence band [36–39]. The first contributions are represented by the wide feature a of the x-ray emission OK_α band and the second contributions by the peak b.

Comparison of the x-ray emission OK_α and TiL_α bands obtained from

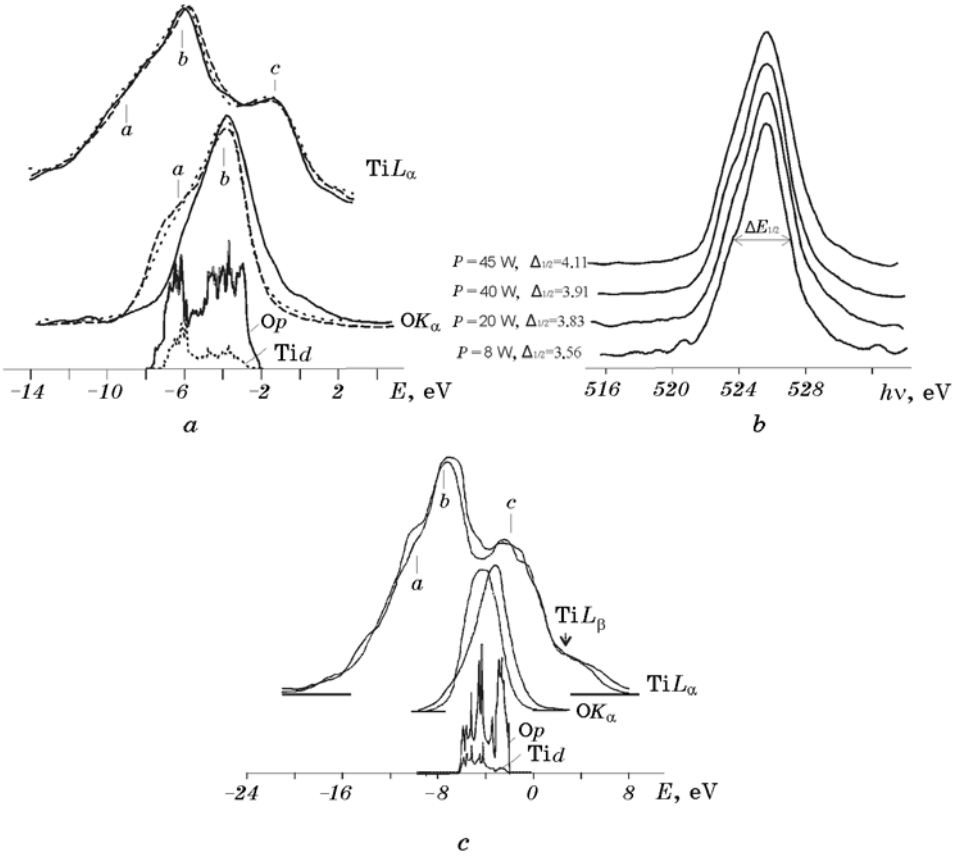

Fig. 3. Comparison on a common energy scale of calculated Tid- and Op-like densities of states and of the x-ray emission TiL_α and OK_α bands of coarse (dashed curves) and nanosize (solid and dotted curves) powders of TiO_2 (a) and $BaTiO_3$ (c): the solid curves are the spectra corresponding to the finest nanopowders with average sizes of 10 nm (TiO_2) and 24 nm ($BaTiO_3$) and the dotted curves are the spectra of TiO_2 nanopowder with size of 107 nm; the x-ray emission OK_α bands of r-TiO_2 nanopowders measured at increasing power of the exciting electron beam (b).

coarse TiO_2 and the nanopowders (Fig. 3, *a*) has revealed that the OK_α band narrows by 0.2–0.5 eV on going from coarse TiO_2 to the nanopowder with average nanoparticle sizes of $\bar{d}$ = 107 nm and by 0.2–1.1 eV when going to the fraction with $\bar{d}$ = 10 nm.

This narrowing is observed in the low-energy part of the OK_α band formed by contributions of the O*p*-bonding states (the feature *a* of the band). The difference square of the OK_α band of coarse TiO_2 and the nanopowder with $\bar{d}$ = 10 nm is many times larger than that of the coarse-grained and nanopowder with the size of $\bar{d}$ = 107 nm. At the same time, the TiL_α band narrowing in the energy region –(6–4) eV is only 0.2–0.3 eV. The ratio of the calculated specific narrowing of the x-ray emission OK_α and TiL_α bands at the intensities corresponding to their maximum narrowing equals to $\eta_{OK_\alpha}/\eta_{TiL_\alpha} = 0.25/0.07 = 3.60 \pm 0.30$, whereas the ratio of the population of the O*p*- and Ti*d*-like states [40] equals to $Q_{Op}/Q_{Tid} = 5.33/1.46 = 3.7$ (this result is in accordance with those described above for *c*-BN, TiC, TiN).

From a comparison of the OK_α bands presented in Fig. 3, *a*, one can see that, like during ultradispersion of covalent-ionic *c*-BN, in a nanopowder of ionic-covalent *r*-TiO_2 the O*p*-states corresponding to the broken bonds of surface atoms concentrate near the top of the valence band, increasing in this energy region the density of the non-bonding O*p*-states. Taking into account the fact that chemical content and the number of the valence electrons in all three powders are exactly the same, the OK_α bands were normalized so that their squares are equal (the method of normalization is similar to that employed in Ref. [41] for XPS spectra). The energy redistribution of the O2*p*-states when going from the coarse-grained to nanopowder TiO_2 should result in significant changes of the band energy of electrons and its contribution to the internal energy of nanopowders. The calculated ratios of the integrals

$$\left(\int_{E_0}^{E_F} I(E) E dE \right)^c \Big/ \left(\int_{E_0}^{E_F} I(E) E dE \right)^n ,$$

where $I(E)$ is proportional to $P(E)N(E)$ in the approximation that $P(E)$ depends weakly upon E and it is similar or equal for these powders, have revealed the increasing of band energy by 3 and 17% when going from coarse TiO_2 to the nanopowders with $\bar{d}$ = 107 and $\bar{d}$ = 10 nm, correspondingly. Consequently, one can assume that significant changes or the appearance of new properties of *r*-TiO_2 are possible when the change in internal energy is sufficient due to changes in band energy because of nanocrystallinity of this material.

The charge states of titanium and oxygen atoms are similar in ionic-covalent perovskite-like $BaTiO_3$ (*p*-$BaTiO_3$) and *r*-TiO_2 compounds, tak-

ing into account XPS measurements of the binding energies of Ti$2p_{3/2}$ and O1s core-level electrons (see Ref. [42]).

However, due to the different geometry of the octahedral surrounding of Ti atoms by oxygen, all the O–O-distances in p-$BaTiO_3$ (0.28327 nm) are greater than the doubled ionic radius of oxygen ($2r_{O^{2-}}$). In contrast, in r-TiO_2 the distances are O–O = 0.25327 nm < $2r_{O^{2-}}$ = 0.270 nm [43, 44]. Therefore, in r-TiO_2, the O–O-bonds exist, and in p-$BaTiO_3$, they are absent.

From a comparison on a common energy scale of the x-ray emission OK_α and TiL_α bands obtained from the coarse and nanosize powders (S_{sp} = 40 m^2/g) with $\bar{d}$ = 24 nm of p-$BaTiO_3$ (Fig. 3, c), it is obvious that the band narrowing occurs in the sequence 'coarse→nanopowder', mainly due to redistribution of the Op- and Tid-states, localized as a result of the Ti–O-bands breaking, towards the higher energies. The Op- and Tid-states in the coarse powder were hybridized [42, 45]. The x-ray emission OK_α band of the coarse $BaTiO_3$ powder does not contain the low-energy subband a, due to the absence of the Op-bonding states involved in the O–O-bonds in this compound. Because of this fact, the OK_α band of the barium titanate coarse powder is symmetric, and its half-width equals to 3.4 eV (the half-width is smaller by 1.0 eV as compared with that of r-TiO_2). The OK_α band of the barium titanate nanopowder is asymmetric, narrowed by 0.2–0.5 eV, and its high-energy contour is shifted by 0.5–0.9 eV as compared with that of coarse-grained $BaTiO_3$. This is due to the fact that, in the $BaTiO_3$ nanopowder after breaking the Ti–O-bonds, the dehybridized Op-states concentrate near the top of the valence band, where according to the calculations [46], the non-hybridized 'pure' non-bonding Op-states are located. The same effect was also observed in the case of ultradispersion of the above-described covalent-ionic c-BN and ionic-covalent r-TiO_2.

However, the main difference in the redistribution of the valence electronic states due to ultradispersion of TiO_2 and $BaTiO_3$ is the fact that, in spite of the resemblance of the shapes of the TiL_α-bands in these compounds, the TiL_α-band of the barium titanate nanopowder narrows by 0.2–1.0 eV in the low-energy region and broadens by 0.3–0.5 eV in the energy region –(5.0–7.0) eV corresponding to the position of the high-energy contour at the main peak b of the band. This is a result of the fact that the population of the Tid + Op-hybrid states in $BaTiO_3$ is significantly higher as compared with that in r-TiO_2 [47].

The calculated integrals ratio

$$\left(\int_{E_0}^{E_F} I(E)EdE\right)^c \Big/ \left(\int_{E_0}^{E_F} I(E)EdE\right)^n$$

for $BaTiO_3$ has revealed that the band energy changes by 11% when going from the coarse powder to the powder with $\bar{d}$ = 24 nm, which is smaller

than that in r-TiO_2 as mentioned above. Therefore, from the above facts, it is obvious that the redistribution of valence electronic states, due to the great contribution of broken bonds in the nanopowders, depends on the character of the chemical bonding and the atomic-crystal structure of materials.

3.4. Dependences of the Cp-State Energy Distribution and of the Shapes of the X-Ray Emission CK_α Band on the Sizes of Carbon Materials

In contrast to crystalline nanopowders, ideal fullerene does not possess broken bonds, and in ideal onions and carbon nanotubes, they exist only on the ends of the nanotubes; the contribution of the broken bonds to the total value of bonds is insignificant in the above materials. At the same time, in nanosize graphene layers which form carbon nanofibres, quantities of the broken and closed bonds are commensurable. Figure 4 presents the x-ray emission CK_α spectra of graphite, onions, nanotubes and nanofibres studied under similar conditions. Figure 4 shows also the CK_α bands of C_{60} and C_{70} investigated in Ref. [48] and obtained in the present work for C_{60} with smaller apparatus distortions ($\Delta E_{ap} \leq 0.2$ eV in the present work and $\Delta E_{ap} = 0.4$ eV in Ref. [48]).

The spectra were compared to elucidate whether the effects of narrowing and changes in the shape of the CK_α bands with decreasing sizes of the carbon materials become apparent and in what way. From the comparison of curves *1* and *2* (Fig. 4), it is obvious that a divided sub-band of the CK_α band of C_{60} is narrower at $I > I_{max}/2$ (by 0.2–0.5 eV) as compared with that of C_{70} in the region of photon energies $h\nu = 274.5$–276.0 eV, and also in the energy region corresponding to contributions of the π-states. The minimum of the CK_α band dividing the pure π-bands (features *e* and *f*) and those mixed with the σ-states in C_{60} is deeper than that in C_{70}, where there is no separation into π_1 (*f*) and π_2 (*e*) sub-bands [49].

The π_1 and π_2 sub-bands are typical for C_{60} due to the difference in the degree of π-overlapping of orbitals above the spherical surface of C_{60} between atoms at the distances of 0.144 and 0.139 nm. The high intensity, symmetry and undivided shape of the π-sub-band in C_{70} are the result of the presence of 8 groups of interatomic distances (0.137 to 0.147 nm), because the degree of π-overlapping of the Cp_z-orbitals in C_{70} does not differ so noticeably as in C_{60}. Such a dispersion of the lengths of σ-bonds leads obviously to a greater width of the sub-band of the CK_α band corresponding to the π + σ-mixed states in C_{70}.

Figure 4, *b* shows a comparison of the CK_α bands of onions (curve *5*), the sizes of which are about 5 nm, and graphite (curve *6*). From the above figure, it is obvious that the CK_α band of the onions is narrower at $I > I_{max}/2$ in comparison with that of graphite, mainly in the energy region where the π and π + σ-bonding states are reflected.

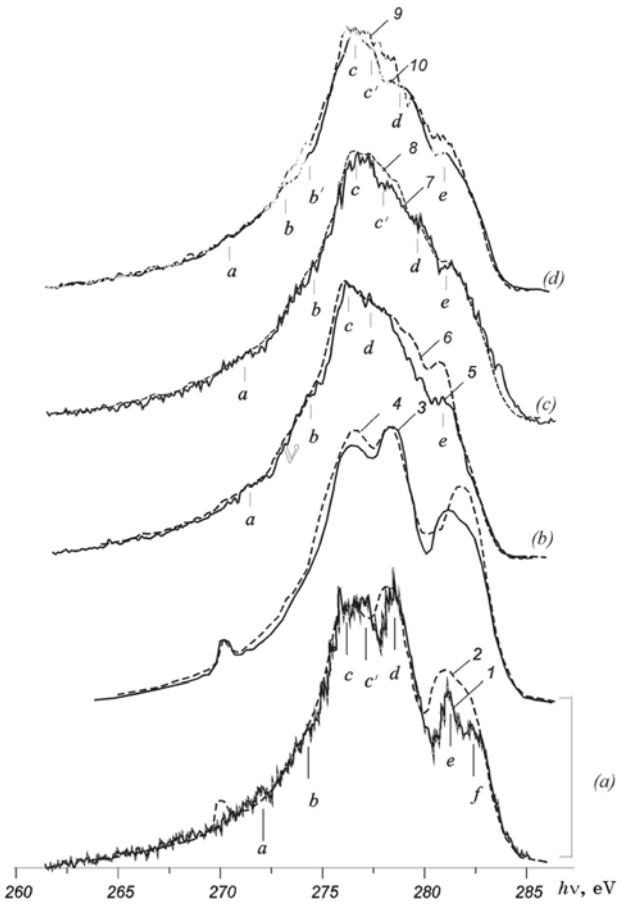

Fig. 4. Comparison of the x-ray emission CK_α bands of carbon nanomaterials: the spectra of C_{60} and C_{70} fullerenes (curve *1* is the spectrum of C_{60} obtained in the present paper, curves *2* and *3* are the spectra of C_{60} and curve *4* is the spectrum of C_{70} obtained in Ref. [48]) (*a*); the spectra of onions (curve *5*) and thermally exfoliated graphite (curve *6*) (*b*); the spectra of nanotubes: double-walled with a diameter 4 nm (curve *7*) and 200-walled with a diameter of 140 nm (curve *8*) obtained in arc discharge by 'MER-corporation' (*c*); the spectra of catalytic nanotubes with diameters of 70 nm (curve *9*) and 20 nm (curve *10*) (*d*).

In the energy region $h\nu$ = 273.0–275.0 eV, corresponding to the sp^2-hybride states of the σ-bonds, the differences are minor. The narrowing of the spectra in the low-energy region is due to the presence of a noticeable quantity of broken bonds due to the fact that spherical sp^2-bonding layers consist of broken, torn or bowed graphene fragments [50]. The greater narrowing in the high-energy part of the CK_α band is a result of breaking the π-bonds between the fragments and decreasing π-overlapping of the C*p*-orbitals above the bowed surface of the fragments.

From the comparison of the CK_α bands (Fig. 4, *c*, curves *7* and *8*) of 200-walled nanotubes with a diameter of 140 nm and double-walled nanotubes with a diameter of 4 nm obtained in arc discharge without catalysts by 'MER-corporation', it is evident that the low-energy contours of the band reveal coincidence.

However, in the high-energy part of the CK_α band where the π- and π+σ-binding states are positioned, the features *c*, *c′* and *d*, *e* reflecting mixed *ppσ* + *ppπ* and pure *ppπ* [51] interactions in the radial planes and along the axis of the nanotubes, respectively, become apparent.

However, the bandwidth of CK_α of double-walled carbon nanotubes

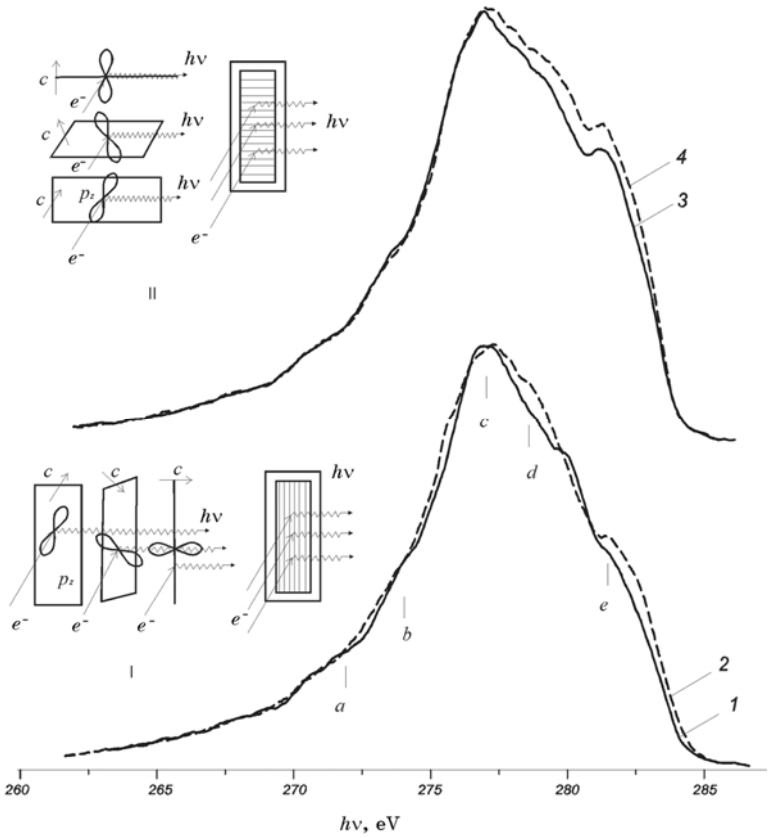

Fig. 5. The x-ray emission CK_α bands of carbon fibres, in orientation I: fibres with a diameter of 30 nm (curve *1*) and 18 μm (*2*), in orientation II: fibres with a diameter of 30 nm (curve *3*) and 18 μm (curve *4*). Note: orientation I: the angle between the direction of x-ray emission and the main direction of the Cp_z-orbitals is in the range of 0–180°; orientation II: the angle between the direction of x-ray emission and the main direction of the Cp_z-orbitals is 90°; *e* are directions of the electron beams; *c* are directions of the axis corresponding to graphene layers; *hν* directions of x-ray emission.

is reduced in comparison with that of the 200-walled nanotubes only near the top of the band (at $I > 0.75 I_{max}$).

This is the result of a decrease of the $\pi + \sigma$-overlapping in the radial plane inside the 200-walled nanotubes with an increase in diameter of every following wall (as a consequence, states involved in such bonds shift towards higher energies).

The comparison of the CK_α spectra of nanotubes with diameters of 70 and 20 nm (Fig. 4, curves *9* and *10*; the latter nanotubes contain many broken bonds after purification from a Co catalyst) reveals that the spectrum width of imperfect nanotubes is reduced in the low-energy and high-energy parts of the CK_α band.

All axes of the p_z-orbitals will be perpendicular to the selection direction of the x-ray, when filaments of the carbon fibres are parallel to it (Fig. 5, orientation II). Therefore, the contribution of the π-bonding p_z-orbitals into the CK_α band intensity is maximum in orientation II, whereas it will be much smaller in orientation I [52]. The comparison of the CK_α spectra of thick (18 μm) and nanosize (30 nm) fibres, obtained for the I- (Fig. 5, curves *1* and *2*) and II-orientations (Fig. 5, curves *3* and *4*), has allowed us to determine qualitatively the ratio of contributions of the broken π- and σ-bonds to the narrowing of the CK_α band when going from thick fibres to nanofibres.

The specific narrowing calculations at $I = 0.86 I_{max}$ (where the narrowings are the greatest at the I- and II-orientations) have shown that $\eta_I \approx \eta_{II} \approx 0.24 \pm 0.01$. This would be expected because the ratio of the number of broken and closed π-bonds does not depend on the fibre orientation. The greater contribution of the σ-states to the emission of the CK_α band at the II-orientation becomes apparent in the narrowing of the band in the low-energy region reflecting the sp^2-hybride σ-bonding states, when going from the thick fibre to the nanofibre. This is the result of the increasing contribution of localized energy levels dehybridized due to sp^2-state bonds breaking.

4. CONCLUSIONS

The effect of the narrowing and changes of the shapes of the x-ray emission bands reflecting the energy distribution of the valence electrons of atoms forming compounds was revealed due to the excitation of x-ray spectra by electron bombardment, which allows refining the nanomaterial surfaces from chemisorbents, when going from bulk to nanomaterials that prove to be common for objects under investigation. This occurs due to the disappearance of splitting of the energy levels of states after the breaking of chemical bonds of the surface atoms, which quantity in nanoparticles is commensurable with the quantity of atoms in their volume.

It was established that the greater population of energy levels of

anions in crystalline compounds causes a greater specific narrowing of the ultrasoft x-ray emission bands radiated by cations and anions. The specific narrowing ratios are close to the ratios of density of electrons concentrated near anions and cations. It was revealed that the energy levels of the states participating in the broken bonds in ionic-covalent crystals are located near the top of the valence bands, increasing their energy and causing an increase in crystal band energy.

As shown, the crystal-structural dependence of the narrowing of the x-ray emission bands and changes of their shapes are related with the change in interatomic distances and the geometry of the nearest surroundings of the atoms emitting spectra. The narrowing and changes of the x-ray emission bands of carbon nanomaterials are greater due to the breaking of π- and σ-bonds as compared with the decreasing degree of π- and σ-overlapping of the Cp_z-orbitals.

REFERENCES

1. V. P. Sachenko, I. I. Geguzin, and V. V. Kolesnikov, *Fiz. Met. Metalloved.*, **44**: 1127 (1997) (in Russian).
2. I. I. Geguzin, A. P. Kovtun, V. P. Sachenko, and I. A. Topol, *Izv. Akad. Nauk SSSR. Ser. Fiz.*, **40**: 288 (1976) (in Russian).
3. M. B. Gordon, F. Cerot-Lackmann, and M. C. Desjonqueres, *Surf. Sci.*, **68**: 359 (1977).
4. R. P. Messemer, S. K. Knudson, and K. H. Johnson, *Phys. Rev. B*, **13**: 1396 (1976).
5. G. P. Borzik, G. A. Katrich, and V. S. Samojlov, *Radiotekhnika i Ehlektronika*, **21**: 1919 (1976) (in Russian).
6. N. Marzari, *MRS Bull.*, **31**: 681 (2006).
7. A. Zunger, A. Franceschetti, G. Bester et al., *J. Phys.: Conf. Ser.*, **46**: 292 (2006).
8. T. Hoshi and T. Fujiwara, *J. Phys.: Condens. Matter*, **18**: 10787 (2006).
9. D. Polder and J. van Santen, *J. Phys.*, **12**: 257 (1946).
10. O. Hunderi, *Phys. Rev. B*, **7**: 3419 (1973).
11. R. Ruppin, *Phys. Rev. B*, **11**: 2871 (1975).
12. M. G. Mason, L. J. Gerenser, and S. T. Lee, *Phys. Rev. Lett.*, **39**: 288 (1977).
13. P. Ascarelli, M. Cini, G. Missoni, and N. Nistico, *J. Phys. (Paris)*, **38**, Suppl. No. 7: C2-125 (1977).
14. C. Senemaud, A. Gheorghiu-De La Rosque, G. Dufour, and N. Herlin, *J. Appl. Phys.*, **84**: 4945 (1998).
15. M. Hävecker, N. Pinna, K. Weiβ et al., *J. Catal.*, **236**: 221 (2005).
16. K. Zhang, X. Sun, G. Lou et al., *Mater. Lett.*, **59**: 2729 (2005).
17. F. Su, L. Lv, and X. S. Zhao, *Int. J. Nanoscience*, **4**: 261 (2005).
18. A. I. Kovalev, D. L. Wainstein, and D. I. Tetelbaum, *Thin Solid Films*, **515**: 591 (2006).
19. Y.-J. Zhu, I. Coulthard, and T. K. Sham, *J. Synchrotron Radiation*, **6**: 529 (1999).
20. Yu. M. Solonin and O. Yu. Khyzhun, *Int. J. Alternat. Energy Ecol.*, **6**: 63 (2002).

21. E. Marino, B. Bouchet-Fabre, D. Porterat, and C. Reynaud, *Diamond Relat. Mater.*, **14**: 1120 (2005).
22. C. Persson, C. L. Dong, L. Vayssieres et al., *Microelectron. J.*, **37**: 686 (2006).
23. O. Vasylkiv and Y. Sakka, *Nano Letters*, **5**: 2598 (2005).
24. E. A. Zhurakovsky, V. I. Trefilov, Ya. V. Zaulychnyy, and G. I. Savvakin, *Dokl. Akad. Nauk SSSR*, **248**: 1360 (1985) (in Russian).
25. J.-Y. Raty, G. Galli, C. Bostedt et al., *Phys. Rev. Lett.*, **90**: 037401 (2003).
26. E. A. Zhurakovsky, Ya. V. Zaulychnyy, V. S. Neshpor et al., *Sov. Powder Metall. Metal Ceram.*, **30**: 64 (1991).
27. Ya. V. Zaulychnyy, *Formation of the Electronic Structure of High-Pressure Phases and Ultradispersive Systems* (Thesis of Disser. for Doctor of Phys.-Math. Sci.) (Kyyiv: I. M. Frantsevych Institute for Problems of Materials Science, N.A.S.U: 2003) (in Ukrainian).
28. O. O. Vasylkiv, *Physical and Chemical Principles of Oxide Nanodispersive Powder Engineering as a Basis of Development of Novel Ceramics* (Thesis of Disser. for Doctor of Tech. Sci.) (Kyyiv: I. M. Frantsevych Institute for Problems of Materials Science, N.A.S.U.: 2006) (in Ukrainian).
29. X. Yong-Nian and W. Y. Ching, *Phys. Rev. B*, **44**: 7787 (1991).
30. V. A. Fomichev and M. A. Rumsh, *J. Phys. Chem. Solids*, **29**: 1015 (1968).
31. E. Tegeler, N. Kosuch, G. Wiech, and A. Faessler, *Phys. Status Solidi B*, **84**: 56 (1977).
32. Ya. V. Zaulychnyy, *Poroshk. Metallurgiya*, No. 9/10: 75 (1999) (in Russian).
33. Ya. V. Zaulychnyy, *Poroshk. Metallurgiya*, No. 7/8: 75 (1999) (in Russian).
34. A. Nekel, P. Rastl, and R. Eibler, *J. Phys. C: Solid State Phys.*, **9**: 579 (1976).
35. A. L. Ivanovsky, V. A. Gubanov, G. P. Shveikin, and E. Z. Kurmaev, *J. Less-Common Met.*, **78**: 1 (1981).
36. Z. Zhang, S.-P. Jeng, and V. Henrich, *Phys. Rev. B*, **43**: 12004 (1991).
37. P. Schelling, N. Yu, and J. Halley, *Phys. Rev. B*, **58**: 1279 (1998).
38. K. M. Glassford and J. R. Chelikowsky, *Phys. Rev. B*, **46**: 1284 (1992).
39. M. Shang-Di and W. Y. Ching, *Phys. Rev. B*, **51**: 13023 (1995).
40. V. A. Veriazov, A. V. Leko, and R. A. Evarestov, *Fiz. Tverd. Tela*, **41**: 1407 (1999) (in Russian).
41. P. J. Hardman, G. N. Raikar, C. A. Muryn et al., *Phys. Rev. B*, **49**: 7170 (1994).
42. L. T. Hudson, R. L. Kurtz, S. W. Robey et al., *Phys. Rev. B*, **47**: 1174 (1993).
43. K. Sugiyama and Y. Takeuchi, *Z. Kristallogr.*, **194**: 305 (1991).
44. J. W. Edwards, R. Speiser, and H. L. Johnston, *J. Am. Chem. Soc.*, **73**: 2934 (1951).
45. D. Bagayoko, G. L. Zhao, J. D. Fan, and J. T. Wang, *J. Phys.: Condens. Matter*, **10**: 5645 (1998).
46. P. Pertosa, *Phys. Rev. B*, **17**: 2011 (1978).
47. O. O. Foya, Ya. V. Zaulychnyy, and V. I. Zarko, *Dopov. NAN Ukr.*, **2**: 82 (2007) (in Russian).
48. J. Kawai and M. Motoyama, *Phys. Rev. B*, **47**: 12988 (1992).
49. J. H. Weaver, J. L. Martins, T. Komeda et al., *Phys. Rev. Lett.*, **66**: 1741 (1991).
50. O. O. Mykhaylyk, Yu. M. Solonin, D. N. Batchelder, and R. Brydson, *J. Appl. Phys.*, **97**: 074302 (2005).
51. D. Östling, D. Tománek, and A. Rosén, *Phys. Rev. B*, **55**: 13980 (1997).
52. W. Burghard, M. Umeno, G. Wiech, and W. Zahorowski, *J. Phys. C: Solid State Phys.*, **16**: 4243 (1983).